A Self-Powered Piezoelectric Energy Harvesting Circuit With an Optimal Flipping Time SSHI and Maximum Power Point Tracking

Liao Wu¹⁰ and Dong Sam Ha¹⁰, Fellow, IEEE

Abstract— This brief presents an ultra low power IC design for piezoelectric (PE) energy harvesting, which integrates a maximum power point tracking (MPPT) circuit and a synchronized switch harvesting on inductor (SSHI) circuit. The proposed circuit also has three different operation modes to extend the range of the harvestable power level generated by a PE transducer. The circuit is designed in CMOS and fabricated in BiCMOS 0.25 μm technology with the die size of 2 mm². The measurement results indicate the circuit can harvest energy with the input power ranging from 10 to 34 μW during MPPT. It achieves peak efficiency of 77% under a PE cantilever voltage of 3.5 V and the battery voltage of 4.2 V.

Index Terms—Vibration energy harvesting, piezoelectric energy harvesting, SSHI, MPPT, FOCV.

I. Introduction

K INETIC energy in the form of vibration or shock is prevalent such as automobiles, airplanes, machinery, and humans. Kinetic energy harvesting with piezoelectric (PE) transducers has been investigated extensively owing to high power density and good scalability of PE devices. A PE cantilever has an internal capacitor C_p , and the charge stored in the C_p poses a unique challenge for PE energy harvesting circuits. The Synchronized Switch Harvesting on Inductor (SSHI) and Synchronous Electric Charge Extraction (SECE) schemes harvest the capacitor charge, and both schemes are based on an LC resonator with an external inductor [1]-[7]. The LC resonator for the SSHI scheme flips the capacitor voltage V_{PZT} [1]–[4]. In contrast, the LC resonator for the SECE scheme transfers the capacitor charge to the inductor temporarily and then to the load [5]-[7]. The SSHI scheme harvests more energy than the SECE scheme for almost all types of PE transducers except those with low coupling coefficients or operating at off-resonant frequencies [7].

Another design issue is impedance matching, which aims to transfer maximum power from a PE transducer to the load.

Manuscript received March 15, 2019; revised May 10, 2019; accepted June 3, 2019. Date of publication June 26, 2019; date of current version September 24, 2019. This work was supported in part by the U.S. National Science Foundation under Award 1704176. This brief was recommended by Associate Editor Y. Lu. (Corresponding author: Dong Sam Ha.)

- L. Wu is with the Department of Electronic Information and Electrical Engineering, Changsha University, Changsha 410022, China.
- D. S. Ha is with the Department of Electrical and Computer Engineering, Virginia Tech, Blacksburg, VA 24061 USA (e-mail: ha@vt.edu).

Color versions of one or more of the figures in this paper are available online at http://ieeexplore.ieee.org.

Digital Object Identifier 10.1109/TCSII.2019.2924963

In fact, as the operating environment of a PE transducer such as operating frequency changes, the source impedance also changes. So a PE energy harvesting circuit needs to keep track of the source impedance and adjust its load impedance accordingly, called maximum power point tracking (MPPT). Two MPPT schemes "Perturb and Observe (P&O)" [8] and "Fractional Open Circuit Voltage (FOCV)" [9]–[11], are most commonly used for PE energy harvesting circuits due to low circuit complexity.

The FOCV scheme disconnects the load periodically and measures the open circuit voltage. Then, it adjusts the load resistance to set the load voltage, i.e., one half of the open circuit voltage. The FOCV scheme leads to low circuit complexity, but energy harvesting is disrupted during the measurement of the open circuit voltage. Lu *et al.* use a bang-bang controller to set its load voltage to the optimal voltage [9]. Shim *et al.* propose a sensing circuit with a small capacitor, which can sample the open circuit voltage in one cycle of the PE transducer [10]. Kawai *et al.* use a peak detector with a small capacitor to shorten the sampling time of the open circuit voltage [11].

The SSHI scheme is effective for small to micro scale PE energy harvesting, and MPPT increases the efficiency of PE energy harvesting over a wide operation range of the PE transducer. Integration of SSHI and MPPT is considered for the PE energy harvesting circuits in [11]–[13]. The circuit in [11] is implemented with discrete components and the one in [12] with a microcontroller. The circuit in [13] shows a simulation model and a flow chart only. This brief presents a PE energy harvesting IC design with SSHI and MPPT. The proposed design adopts our previous SSHI circuit presented in [4] and the FOCV scheme for MPPT. In addition, the circuit has three different operation modes to extend the range of the harvestable power level.

This brief is organized as follows. Section II reviews our previous SSHI circuit adopted for the proposed design. Section III explains operation of the proposed circuit. Section IV describes implementation of major building blocks. Section V presents experimental results and compares the performance of competing designs. Section VI draws a conclusion.

¹It assumes that the vibration amplitude of a PE transducer remains the same even if the load is disconnected. In general, it is true for a PE transducer with a low coupling coefficient or vibrating at off-resonant frequencies [14].

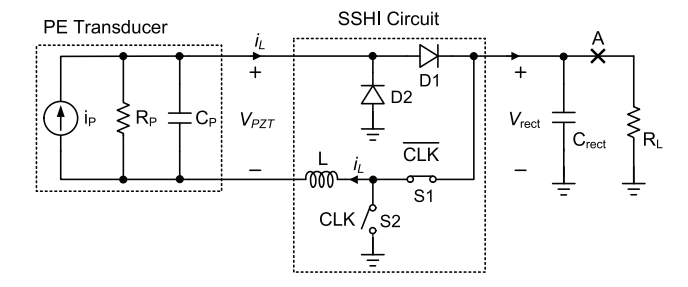


Fig. 1. A conceptual circuit diagram of the SSHI circuit in [4].

II. Preliminaries

A. Review of the SSHI Circuit

The proposed circuit incorporates MPPT to our existing SSHI circuit in [4]. The conceptual circuit diagram of the SSHI circuit, specifically with the series SSHI configuration, is shown in Fig. 1. Consider the current of the PE transducer crosses from positive to negative at time t_0 , while the switch S1 is open and S2 closed. Now, S1 closes and S2 opens as shown in the figure, an LC resonant circuit is formed through L, C_p , D1, and S1. The capacitor voltage V_{PZT} starts to oscillate. In order to maximize the flipped capacitor voltage from positive to negative, the switch S1 should be open at the optimal time t_{opt} , in which V_{PZT} becomes peak in the negative voltage. The controller for a conventional SSHI circuit without the diode D1 is complicate to result in large power dissipation. However, addition of the diode D1 allows the switch S1 to open at any time after t_{opt} , which simplifies the controller. The diode D2 performs the same role when the current i_p crosses from negative to positive. It should be noted that the SSHI circuit also performs rectification of the voltage. For details of the operation, refer to [4].

B. Maximum Power Point Tracking for the SSHI Circuit

As the operating condition such as the vibration frequency of a PE transducer changes, the source impedance of the PE transducer also changes to require MPPT. Incorporation of MPPT to our SSHI circuit in Fig. 1 is the focus of the proposed circuit. After completing the voltage flipping, the SSHI circuit in Fig. 1 can be modeled as the inductor L alone assuming ideal switches and diodes, which is connected in series with the PE transducer. So, the PE transducer in series with L is the source as far as the FOCV scheme is concerned. The load for the FOCV scheme is a boost converter. Hence, the FOCV scheme disconnects the point "A" in Fig. 1 periodically and measures the open circuit voltage V_{rect} for the proposed circuit. The switching frequency of the booster converter is adjusted through pulse skipping modulation (PSM), which sets the input voltage of the converter, equally the load voltage, to the optimal voltage.

III. OPERATION OF THE PROPOSED CIRCUIT

The proposed circuit aims to harvest a sub-mW range ultra low power. The major contribution of this brief is addition of the MPPT capability to our SSHI circuit in [4]. Three operation modes are also incorporated to lower the harvestable input power level and hence to increase the net energy delivered to the battery.

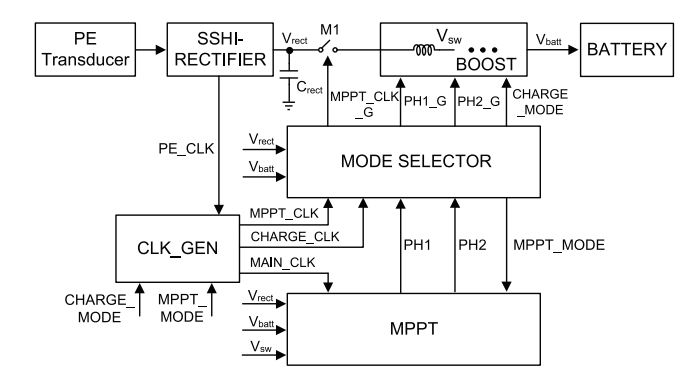


Fig. 2. Block diagram of the proposed PE energy harvesting circuit.

A. Block Diagram

Fig. 2 shows the block diagram of the proposed circuit. The "SSHI-RECTIFIER" block is essentially the same as our SSHI circuit in [4]. A boost converter boosts the rectifier output voltage V_{rect} to charge the battery with nominal charging voltage of 4.2 V. The "MODE SELECTOR" block selects an appropriate mode depending on the power level generated by the PE transducer and the charge level of the battery. The MPPT block senses the open circuit voltage V_{rect} of the "SSHI-RECTIFIER" block, while the boost converter being disconnected, and adjusts the duty cycle of the converter to set V_{rect} one half of the open circuit voltage.

B. Operation Modes

The proposed circuit has three different operation modes, named LOW_POWER, CHARGE, and MPPT, based on the output voltage V_{rect} of the "SSHI-RECTIFIER" block and the battery voltage V_{batt} . The circuit enters to the LOW_POWER mode if the input power generated by the PE transducer is too low to charge the battery, equivalently V_{rect} is below a certain preset level. Both the boost converter and the MPPT block are turned off to save power. The circuit enters to the CHARGE mode if V_{rect} is above the preset level, but the battery voltage V_{batt} is still too low to power the MPPT block. The boost converter is activated to charge the battery, but the MPPT block remains deactivated. Finally, it enters to the MPPT mode if both V_{rect} and V_{batt} are above the preset levels. The MPPT block powered by the battery is activated and performs MPPT.

IV. IMPLEMENTATION OF THE PROPOSED CIRCUIT

This section describes an IC implementation of the proposed PE energy harvesting circuit. The major design issues lie in the interface for the boost converter, the MPPT block, and the "MODE SELECTOR" block, which are explained below. The "SSHI-RECTIFIER" and "CLK_GEN" blocks in Fig. 2 are not covered to save space. (Refer to [4] for the "SSHI-RECTIFIER" block.) The entire circuit was designed and fabricated in a 0.25 μ m BiCMOS technology, where only CMOS devices were used for the proposed circuit.

A. Boost Converter

Fig. 3 shows a boost converter and its interface. During the CHARGE mode, the switch M1 is closed to connect

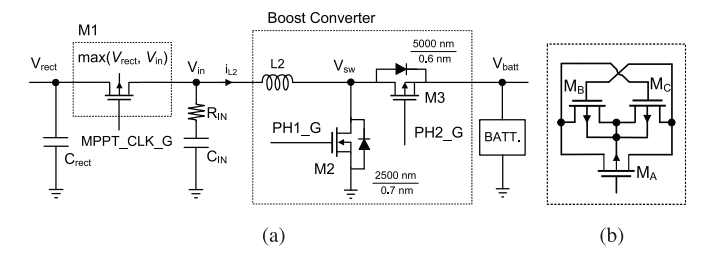


Fig. 3. Boost converter (a) with its interface (b) implementation of M1.

the booster converter to the "SSHI-RECTIFIER". The driving signal PH1_G for M2 operates the boost converter in the discontinuous conduction mode (DCM) with a fixed frequency of 4 kHz and a fixed duty cycle of 4%. Synchronous operation of the converter in DCM requires a zero crossing detector, whose power dissipation decreases the net energy harvested for the available input energy level. To address the problem, the boost converter is configured to *asynchronous* in the CHARGE mode and relies on the body diode of M3 while M3 being turned off. It is accomplished by setting the driving signal PH2_G to high. It should be noted that the signal PH1_G (PH2_G) is the same as PH1 (PH2), but delayed by the associated gate driver.

During the MPPT mode, the boost converter is configured into synchronous, i.e., both M2 and M3 are switching. It adopts constant on-time pulse frequency modulation based on the pulse skipping scheme. The output voltage V_{rect} of the "SSHI-RECTIFIER" block can vary largely depending on the available input energy level. Hence, it is not guaranteed that V_{rect} is always greater than V_{in} . To prevent reverse flow of the current through the body diode, the switch M1 is implemented using three PMOS transistors [15]. The two cross-coupled PMOS transistors, M_B and M_C , ensure the bulk of M_A is connected to the higher voltage between V_{rect} and V_{in} , and hence the body diode is turned off. The off-chip RC filter formed of R_{IN} (= 5 Ω) and C_{IN} (= 50 nF) at the output of M1 suppresses the surge of V_{in} as the M1 closes periodically during the MPPT mode.

B. MPPT Block

Fig. 4 shows the MPPT circuit with the MAIN_CLK signal of 90 kHz. The sampler consists of two identical resistors R1 and R2, the switch M4, and the capacitor C1. As the MPPT_CLK_G signal becomes high, the switch M1 shown in Fig. 3 opens and the switch M4 closes. The load or the boost converter is disconnected, and so V_{rect} becomes the open circuit voltage. The capacitor C1 holds the optimal voltage $0.5V_{rect}$, denoted as V_{rect_opt} . Note that the optimal voltage $0.5V_{rect}$ can readily be set to a different voltage by changing the resistors values of R1 and R2.

When MPPT_CLK_G becomes 0, M1 closes to connect the load, and M4 opens for C1 to hold V_{rect_opt} . The comparator COMP1 compares V_{rect} with the optimal value V_{rect_opt} at the rising edge of CLK_C clock. If V_{rect} is greater than the optimal value, it generates a pulse PH1, which in turn triggers to generate a PH2 pulse. PH1 and PH2 pulses switch the boost converter to transfer the energy stored in C_{rect} in Fig. 3 to the

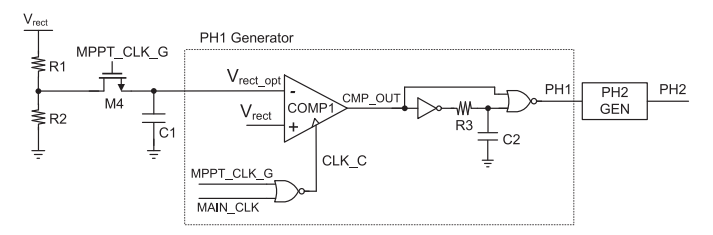


Fig. 4. Core circuit for the FOCV scheme and the PH1 generator.

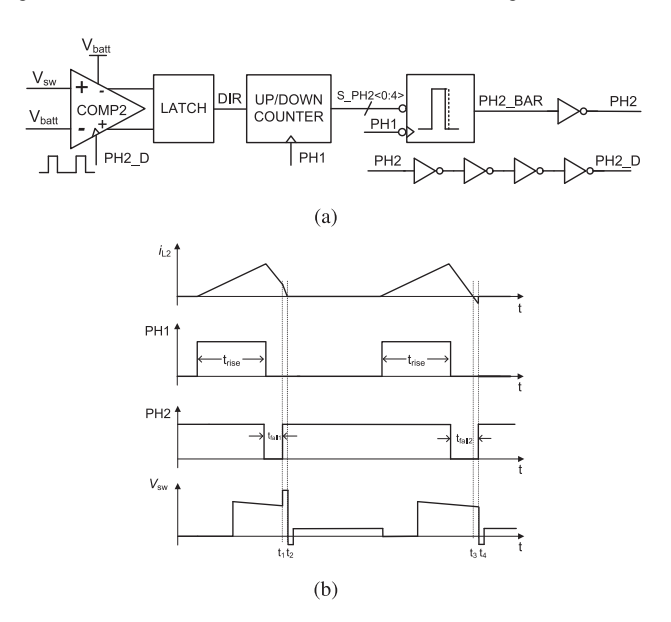


Fig. 5. PH2 generator (a) circuit (b) relevant waveforms.

battery, resulting in decrease of the voltage V_{rect} . If V_{rect} is smaller than the optimal value, PH1 and PH2 pulses are not generated, resulting in pulse skipping modulation. The booster becomes inactive, and the harvested energy is accumulated at C_{rect} to increase V_{rect} . The DCM operation necessitates a ZCD (zero crossing detector) to identify finishing point of the PH2 pulse. We adopt a closed-loop DCM scheme to eliminate a power hungry ZCD [16]. Fig. 5 shows the PH2 generator and its associated waveforms. A falling edge of the PH1 signal triggers generation of a PH2 pulse, whose width is decided by the 5-bit counter value. Suppose that the off time of the PH2 pulse is shorter than desired one as shown for the case of t_{fall1} in Fig. 5 (b). The inductor current is not discharged completely and keeps on flowing through the body diode of M3 in Fig. 3. It implies V_{SW} in Fig. 3 becomes higher than V_{batt} , and the comparator output COMP2 becomes high (rather than zero) at the rising edge of PH2_D. It implies that the off-time pulse width of PH2_D is shorter. It sets the following latch high, which in turn increases the counter by 1 at the beginning of the next cycle and hence the off-time pulse width of PH2 by one unit. The opposite procedure happens if the off-time pulse width of PH2_D is too long as shown for the case of t_{fall2} in the waveform. The pulse width of PH2 converges to the target value within the margin of 40 ns for the proposed circuit.

C. Mode Selector

The threshold voltage of V_{rect} is set to 2 V for the proposed design, and that for the V_{batt} 2.5 V. Fig. 6 shows the core part

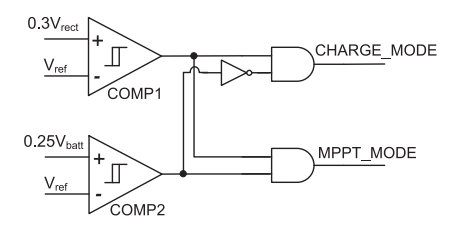


Fig. 6. Mode signal generator.

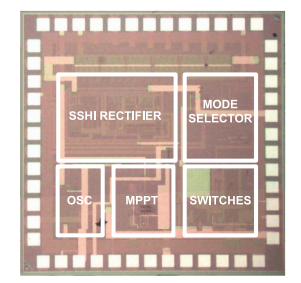


Fig. 7. Die photo.

of the mode selector, which is powered by V_{rect} . It senses two voltages, V_{rect} and V_{batt} , and scales down them to $0.3V_{rect}$ and $0.25V_{batt}$, respectively, with resistor dividers. Two comparators with hysteresis compare the scaled down voltages with a reference signal V_{ref} of 0.6 V. (The reference voltage V_{ref} can be adjusted externally for the proposed circuit.)

V. MEASUREMENT RESULTS

The proposed circuit was implemented and fabricated only in CMOS in 0.25 μm BiCMOS technology. Fig. 7 shows the die photograph of the test chip. The total area is 2 mm², of which the SSHI-RECTIFIER occupies the largest area of 0.63 mm².

A PE cantilever with tip mass of 1 gram is mounted on the base of a shaker. The C_P (=19 nF) and R_P (=600 k Ω) values of the equivalent circuit model in Fig. 1 were obtained from the PE cantilever through measurements. Major off-chip components of the circuit are two inductors, the SSHI inductor in Fig. 1 and the power stage inductor, of 220 μ H each, and the capacitor C_{rect} of 500 nF. The measurement results are given below. The vibration frequency of the PE cantilever is set to 140 Hz in the experiments unless stated otherwise.

The first experiment verifies the operation of the FOCV and MPPT schemes in the MPPT mode. We increased the acceleration of the PE cantilever vibration from 0.23 g to 0.3 g and then back to 0.23 g in the experiment. Fig. 8 shows voltage waveforms of the PE cantilever voltage, MPPT_CLK_G signal, and the output voltage V_{rect} . (Refer to Fig. 3 and Fig. 4 for the voltages and the signal.) As the acceleration increases from 0.23 g to 0.3 g, the peak voltage of the PE cantilever V_{PZT} increases from 1.6 V to 3.9 V momentarily and then settles to 2.2 V, and V_{rect} rises from 1.52 V to 3.84 V momentarily and then settles to 1.92 V. An MPPT_CLK_G pulse with the duty cycle of 1.56% is generated once in every 2046 vibration periods of the PE cantilever or 14.6 seconds. When the MPPT_CLK_G signal becomes high momentarily, the load is

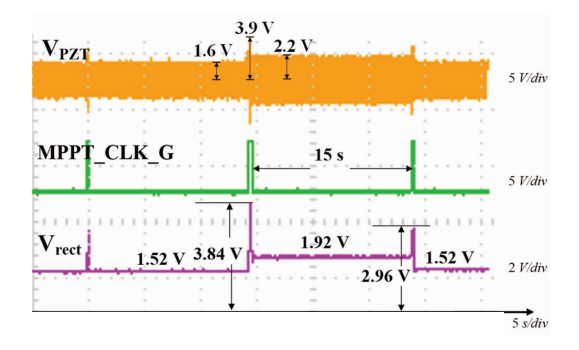


Fig. 8. Measured waveforms of relevant signals during steady-state of the MPPT mode.

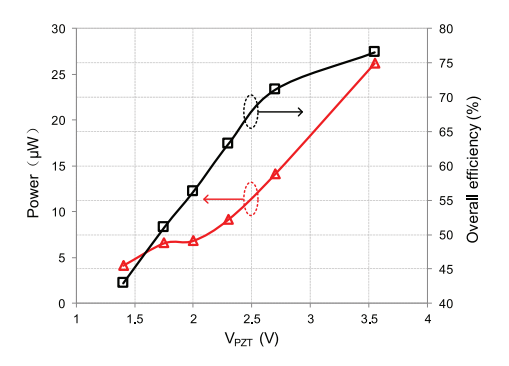


Fig. 9. Harvested power and the system efficiency.

disconnected. V_{PZT} shoots up to 3.9 V nearly instantly, and V_{rect} to 3.84 V, which is, in fact, the open circuit voltage. As the MPPT_CLK_G signal goes back to zero, and the load is reconnected, V_{rect} becomes 1.92 V or one half of the open circuit voltage, implying the impedance matching. When the acceleration changes from 0.3 g to 0.23 g, the open circuit voltage of V_{rect} is 2.96 V. However, when the load is reconnected, V_{rect} becomes 1.52 V, a slightly larger than one half of the open circuit voltage, implying slight mismatch.

Fig. 9 shows the output power and efficiency of the proposed circuit during the MPPT mode. The V_{PZT} voltage is controlled by changing the acceleration of the PE cantilever vibration, and battery voltage is set to 4.2 V initially. The output power denotes the power flowing into the battery, and the efficiency is defined as the ratio of the output power to the input power or the power delivered from the PE transducer. As expected, the output power and the efficiency increase as V_{PZT} increases and the output power reaches 26 μ W for V_{PZT} of 3.5 V with the efficiency of 77%. The output power and efficiency would increase as the voltage increases further, but higher voltages are not tried due to the limit of the breakdown voltage (= 7 V) of the MOSFETs used for the proposed circuit. The low efficiency at the low voltage range of V_{PZT} is mainly due to reduced efficiency of the SSHI operation and relative increase of the switching losses of the power transistors. Finally, we observed the circuit was able to cold-start even if the capacitor C_{rect} and the battery were completely discharged.

Table I summarizes the performance and characteristics of recent, state-of-the-art PE energy harvesting circuits with MPPT. It is difficult to make a fair comparison of the performance due to differences such as processing technology,

Publication	TVLSI 2011 [9]	TPE 2012 [8]	JSSC 2015 [10]	IECON 2015 [11]	This work
Process	$0.35~\mu\mathrm{m}$	Discrete	$0.35~\mu\mathrm{m}$	Discrete	$0.25~\mu\mathrm{m}$
	CMOS	Components	BCDMOS	Components	BiCMOS
MPPT	FOCV	P&O	FOCV	FOCV	FOCV
SSHI	No	No	No	SSHI	SSHI
Power management scheme	e No	No	No	No	Yes
Cold start capability	Yes	Yes	Yes	No	Yes
Power dissipation	\sim 3.8 μW (for $i_P = 152 \ \mu A$) \sim 11 μW (for $i_P = 264 \ \mu A$)	\sim 1.5 mw	-	-	7.2 µW
Peak efficiency (%)	96†	76†	72	_	77
FoM (%)	0.98 (for $i_P = 152 \ \mu A$) 0.96 (for $i_P = 264 \ \mu A$)	0.71	1.09††	_	1.70

TABLE I
COMPARISONS OF RECENT PE ENERGY HARVESTING CIRCUITS WITH MPPT

PE transducer type, power and voltage levels. Further, since the objective of MPPT is to achieve high efficiency for a wide operating range at the cost of reduced peak efficiency, comparison of performance only at peak performance points fails to reflect MPPT performance. Having noted it, the figure of merit (FoM) in (1) is often used to compare the performance of PE energy harvesting circuits [6]. The FOM compares the measured power P_{out} delivered to the load against the power delivered to the optimal resistive load connected to the PE transducer through an ideal full-bridge rectifier.

$$FoM = \frac{P_{out}}{f_P C_P V_{oc}^2} \tag{1}$$

The proposed circuit achieves the highest FOM of 1.7 among the circuits, which is mainly attributed to adoption of the SSHI scheme. The circuit in [11] also adopts SSHI, but is implemented with discrete components and a microcontroller. Hence, the FOM would be low due to relatively large power dissipation to result in small P_{out} . The power efficiency of the proposed circuit is 77%, and that for [10] is 72%. The power efficiency of [9] is 96%, but it does not consider the power dissipation of the rectifier.

VI. CONCLUSION

This brief presents a PE energy harvesting IC design with MPPT and SSHI based on our previous SSHI circuit presented in [4]. The proposed circuit is fabricated in a BiCMOS 0.25- μ m technology, and it achieves the peak efficiency of 77% and the highest FOM of 1.7 among competing circuits.

REFERENCES

- D. A. Sanchez, J. Leicht, F. Hagedorn, E. Jodka, E. Fazel, and Y. Manoli, "A parallel-SSHI rectifier for piezoelectric energy harvesting of periodic and shock excitations," *IEEE J. Solid-State Circuits*, vol. 51, no. 12, pp. 2867–2879, Dec. 2016.
- [2] M. Dini, A. Romani, M. Filippi, and M. Tartagni, "A nanopower synchronous charge extractor ic for low-voltage piezoelectric energy harvesting with residual charge inversion," *IEEE Trans. Power Electron.*, vol. 31, no. 2, pp. 1263–1274, Feb. 2016.

- [3] A. M. Eltamaly and K. E. Addoweesh, "A novel self-power SSHI circuit for piezoelectric energy harvester," *IEEE Trans. Power Electron.*, vol. 32, no. 10, pp. 7663–7673, Oct. 2017.
- [4] L. Wu, X.-D. Do, S.-G. Lee, and D. S. Ha, "A self-powered and optimal SSHI circuit integrated with an active rectifier for piezoelectric energy harvesting," *IEEE Trans. Circuits Syst. I, Reg. Papers*, vol. 64, no. 3, pp. 537–548, Mar. 2017.
- [5] P. Gasnier et al., "An autonomous piezoelectric energy harvesting IC based on a synchronous multi-shot technique," *IEEE J. Solid-State Circuits*, vol. 49, no. 7, pp. 1561–1570, Jul. 2014.
- [6] D. Kwon and G. A. Rincón-Mora, "A single-inductor 0.35 μm CMOS energy-investing piezoelectric harvester," *IEEE J. Solid-State Circuits*, vol. 49, no. 10, pp. 2277–2291, Oct. 2014.
- [7] T. Hehn *et al.*, "A fully autonomous integrated interface circuit for piezoelectric harvesters," *IEEE J. Solid-State Circuits*, vol. 47, no. 9, pp. 2185–2198, Sep. 2012.
- [8] N. Kong and D. S. Ha, "Low-power design of a self-powered piezoelectric energy harvesting system with maximum power point tracking," *IEEE Trans. Power Electron.*, vol. 27, no. 5, pp. 2298–2308, May 2012.
- [9] C. Lu, C.-Y. Tsui, and W.-H. Ki, "Vibration energy scavenging system with maximum power tracking for micropower applications," *IEEE Trans. Very Large Scale Integr. (VLSI) Syst.*, vol. 19, no. 11, pp. 2109–2119, Nov. 2011.
- [10] M. Shim, J. Kim, J. Jeong, S. Park, and C. Kim, "Self-Powered 30 μW to 10 mW piezoelectric energy harvesting system with 9.09 ms/V maximum power point tracking time," *IEEE J. Solid-State Circuits*, vol. 50, no. 10, pp. 2367–2379, Oct. 2015.
- [11] N. Kawai, Y. Kushino, and H. Koizumi, "MPPT controlled piezoelectric energy harvesting circuit using synchronized switch harvesting on inductor," in *Proc. IEEE Ind. Electron. Soc. (IECON)*, Yokohama, Japan, Nov. 2015, pp. 1121–1126.
- [12] Z. J. Chew and M. Zhu, "Combined power extraction with adaptive power management module for increased piezoelectric energy harvesting to power wireless sensor nodes," in *Proc. IEEE SENSORS*, Orlando, FL, USA, Nov. 2016, pp. 1–3.
- [13] M. Zouari, S. Naifar, G. Bouattour, N. Derbel, and O. Kanoun, "Energy management based on fractional open circuit and P-SSHI techniques for piezoelectric energy harvesting," *tm Technisches Messen*, vol. 86, no. 1, pp. 14–24, Jan. 2019.
- [14] S. Priya et al., "A review on piezoelectric energy harvesting: Materials, methods, and circuits," Energy Harvesting Syst., vol. 4, no. 1, pp. 3–39, Mar. 2017.
- [15] M. Ghovanloo and K. Najafi, "Fully integrated wideband high-current rectifiers for inductively powered devices," *IEEE J. Solid-State Circuits*, vol. 39, no. 11, pp. 1976–1984, Nov. 2004.
- [16] E. J. Carlson, K. Strunz, and B. P. Otis, "A 20 mV input boost converter with efficient digital control for thermoelectric energy harvesting," *IEEE J. Solid-State Circuits*, vol. 45, no. 4, pp. 741–750, Apr. 2010.

[†] It does not consider the power dissipation of the rectifier.

 $^{^{\}dagger\dagger}$ It is calculated for the PE transducer open-circuit voltage of 2 V.